

X-ray variability of σ Orionis young stars as observed with *ROSAT*

J. A. Caballero¹, J. López-Santiago, E. de Castro and M. Cornide
*Departamento de Astrofísica y Ciencias de la Atmósfera, Facultad de Física,
 Universidad Complutense de Madrid, E-28040 Madrid, Spain*
 caballero@astrax.fis.ucm.es

ABSTRACT

We used the Aladin Virtual Observatory tool and High Resolution Imager *ROSAT* archival data to search for X-ray variability in scale of days in 23 young stars in the σ Orionis cluster and a background galaxy. Five stars displayed unambiguous flares and had probabilities $p_{\text{var}} \gg 99\%$ of being actual variables. Two of the detected flares were violent and long-lasting, with maximum duration of six days and amplitude of eight times above the quiescent level. We classified another four stars as possible X-ray variables, including the binary system formed by the B2Vp star σ Ori E and its close late-type companion. This makes a minimum frequency of high-amplitude X-ray variability in excess of a day of 39 % among σ Orionis stars. The incidence of this kind of X-ray variability seems to be lower among classical T Tauri stars with mid-infrared flux excesses than among fast-rotating, disk-less young stars.

Subject headings: open clusters and associations: σ Orionis — stars: activity — X-ray: stars

1. Introduction

The σ Orionis cluster ($\tau \sim 3$ Ma, $d \sim 385$ pc) is routinely investigated for deriving basic properties associated to the star formation process: initial mass function, frequency of disks, or incidence of X-ray emission (Caballero 2008b; Walter et al. 2009). In particular, the X-ray emission from early- and late-type cluster stars have been investigated by a number of authors (Wolk et al. 1996; Sanz-Forcada et al. 2004; Franciosini et al. 2006; Skinner et al. 2008; López-Santiago & Caballero 2008 and references therein). However, the X-ray variability in the cluster, which informs on the frequency of flares, strength of magnetic fields, evolution of angular momenta, variations in the radiative wind shocks, or presence of a low-mass companion, has been mostly studied in relatively short time scales, of up to 24 h (with *XMM-Newton* and *Chandra*; references above). Only Berghöfer & Schmitt (1994) and Groote & Schmitt

(2004) have carried out mid-term X-ray variability studies in σ Orionis (about 75 ks distributed over more than 30 days), but just of the two brightest stars: σ Ori AF–B (O9.5V + B0.0V + B0.5V) and σ Ori E (B2Vp + ?). Here we revisit *Röntgensatellit* (*ROSAT*) data to search for X-ray variability of σ Orionis stars in time scales of days.

2. Analysis

2.1. *ROSAT*, HRI, and 1RXH

ROSAT (Jun 1990–Feb 1999) was a joint German, US, and UK space telescope designed for measurement of soft X-rays in the energy range of 0.1–2.4 keV, corresponding to wavelengths of about 120–6 Å. One of its focal plane instruments was the *ROSAT* High Resolution Imager (HRI), which provided simultaneously relative large field of view (38×38 arcmin²) and good spatial resolution (0.499 ± 0.001 arcsec pixel⁻¹, FWHM ~ 2 arcsec). However, HRI had negligible energy resolution.

In this work, we used the *ROSAT* Source Cat-

¹Investigador Juan de la Cierva at the UCM.

alog of Pointed Observations with HRI (1RXH; *ROSAT* Consortium 2000)¹. This catalog contains a list of sources detected by the Standard Analysis Software System in reprocessed, public HRI datasets. In addition to a set of source and sequence flags provided by the *ROSAT* data centers in Germany, the US, and the UK, each source in the catalog has associated basic parameters like coordinates, count rate, or signal-to-noise ratio. Regrettably, although exposure time is given with an accuracy of 1 s, dates of observation start and finish (labels `begDate` and `endDate`) are provided in “Y:M:D” mode (date expressed as year, month number, day in month; e.g. “1995-02-26”). As a result, the 1RXH time resolution is of *one day*. Since we were interested in a qualitative estimation of variability in scales of days, having a larger precision was unnecessary.

2.2. Aladin and 1RXH

We loaded all the X-ray 1RXH events at less than 30 arcmin to σ Ori AF–B with the Aladin sky atlas (Bonnarel et al. 2000; Caballero 2009). For an easier visualization, we overimposed the 1976 detected events onto a digitized image (Fig. 1).

In the 1RXH catalog, there are some single events at angular separations larger than 30 arcmin to σ Ori AF–B, but they are embedded in the nearby Horsehead Nebula and Flame Nebula molecular clouds. The area investigated by us is, however, nearly free of absorption. Sherry et al. (2008) derived $A_V = 0.19 \pm 0.02$ mag by comparing the observed $B - V$ color of a number of stars with the expected $(B - V)_0$ for each star’s spectral type. Besides, in the light of some studies of the spatial distribution and kinematics in the cluster, stars at more than 30 arcmin to the σ Orionis center have low probabilities to belong to the cluster (Jeffries et al. 2006; Caballero 2007a, 2008a).

HRI observations were carried out during two intervals spaced almost three years. The temporal distribution of the observations is illustrated in Fig. 2. The main run consisted of one *ROSAT* visit per day during 34 days from 1995 Feb 26 to 1995 Mar 31 (PI: J. H. M. M. Schmitt). The other run consisted of a single observation on 1992 Sep 13. Except for the 1995 Mar 15 observation, which lasted for only 0.22 ks, individual

“exposure live times” during the main run varied in the approximate time interval 1.0–3.6 ks, with mean and standard deviation $\text{ExpTime} = 2.2 \pm 0.7$ ks. However, the 1992 Sep 13 observation was longer and lasted for more than 4 h ($\text{ExpTime} \approx 14.6$ ks).

We complemented the temporal information above with that provided by the *ROSAT* Mission web page at the Max-Planck-Institut für extraterrestrische Physik (MPE)². The time spanning between start and end of daily observations were in general larger than ExpTime . For example, total pointing time in 1995 Feb 26 was 2.707 ks, but the HRI detector was switched off in three occasions for a summed time interval of 0.342 ks, thus giving $\text{ExpTime} = 2.365$ ks. However, only in a few cases total pointing time was significantly (by a factor at least two) larger than ExpTime .

All pointing coordinates were identical. Since the *post facto* attitude determination accuracy of *ROSAT* was 6 arcsec, the overlapping field of view between different pointings was maximal (i.e. the full 38 arcmin-size square centered on σ Ori AF–B). Therefore, all sources were observed (or at least pointed at) in each of the observations. Besides, the processing site of all images was the MPE, which ensures the homogeneity of the dataset.

2.3. Optical/near-infrared counterparts

We identified 24 groups of 1RXH events, each of them having more than 20 associated 1RXH events, N (i.e. $N > 20$). Due to the clear radial concentration of events (see below) and small size ($\rho < 10$ arcsec) of each group in comparison to their mutual separation ($\rho > 40$ arcsec), we found no problem to associate a group of 1RXH events to every single X-ray source. For an accurate follow-up analysis, we only selected X-ray sources with more than 20 events. Two discarded *ROSAT* X-ray sources with lower number of events are linked to the σ Orionis stars Mayrit 403090 ([W96] 4771–1038; $N = 15$) and Mayrit 374056 ([W96] 4771–1075; $N = 15$). Remaining discarded X-ray sources have 11 or less associated 1RXH events.

Then, we searched with Aladin for the optical and near-infrared counterparts of the X-ray

¹<http://cdsarc.u-strasbg.fr/viz-bin/Cat?IX/28A>

²<http://www.mpe.mpg.de/xray/wave/rosat/index.php?lang=en>

sources with $N > 20$. The basic properties of the 24 identified X-ray sources and their corresponding optical/near-infrared counterparts are given in Tables 1 and 2. All except one counterpart are σ Orionis cluster members in the Mayrit catalog (Caballero 2008b). The cluster non-member is a galaxy with a very strong X-ray emission already detected by the *Einstein Observatory*, 2E 1456 (Section 3.1.6).

On the one hand, in Table 1 we provide the means and standard deviations of the right ascension and declination ($\bar{\alpha}$, $\bar{\delta}$, σ_α , σ_δ), number of associated events (N), mean and standard deviation of the net count rate (\overline{CR} , σ_{CR}), and mean of the error on the count rate ($\overline{\delta CR}$) of each group of 1RXH events associated to an X-ray source. In the antepenultimate column, we list a normalized double-weighted χ^2 of the X-ray series computed as in Fuhrmeister & Schmitt (2003; see Section 2.4)³:

$$\chi^2 = \frac{1}{N} \sum \frac{(\overline{CR} - CR_i)^2}{\delta CR_i^2}. \quad (1)$$

The time series (or “light curves”) of the 24 X-ray sources are shown in Figs. 7 to 14. For the typical length of an individual observation, $\text{Exptime} \approx 2.2\text{ks}$, the faintest sources with $\overline{CR} = 5\text{--}10\text{ks}^{-1}$ have corresponding low total (source + background) counts within the radius of source circle for intensity measurement, of about 10–20 counts in each of the short observations. In occasions, these sources were too faint even to be detected. Likewise, there may be several events associated to a bright X-ray source for each daily observation ($\dot{N} \sim 4.8\text{d}^{-1}$ for the brightest ones).

On the other hand, in Table 2 we provide the recommended alternative names, Two-Micron All Sky Survey (2MASS) coordinates and J -band magnitudes, and remarks from the literature for the optical/near-infrared counterparts of the X-ray sources in Table 1. Deep Near Infrared Survey of the Southern Sky (DENIS) i and 2MASS HK_s magnitudes of the sources were tabulated in the Mayrit catalog (Caballero 2008b).

As can be seen in Table 1, the accuracy of the astrometry of the X-ray sources, quantified by the

standard deviations σ_α and σ_δ , varies with the distance to the instrument axis (i.e. the center of the field of view) from $\sim 1.5\text{arcsec}$ for σ Ori AF–B to $\sim 4.8\text{arcsec}$ for Mayrit 969077 (at $\rho \approx 969\text{arcsec} \approx 16.2\text{arcmin}$, $\theta \approx 77\text{deg}$, to σ Ori AF–B). This variation is due to the well-known degradation of the point spread function with the distance to the instrument axis of *ROSAT* in particular and of all X-ray missions in general. In any case, our spatial resolution of 2–4 arcsec after averaging is comparable to that one of a single *XMM-Newton* pointing in σ Orionis (Watson et al. 2003, 2009; Franciosini et al. 2006; López-Santiago & Caballero 2008).

We are confident of our identification of optical counterparts. The separation between the X-ray sources and their respective optical counterparts, illustrated in Fig. 3, is null within uncertainties ($\Delta\alpha = -0.7 \pm 1.7\text{arcsec}$, $\Delta\delta = +0.9 \pm 1.7\text{arcsec}$). All of them except Mayrit 750107 had been tabulated by Caballero (2008b) as strong X-ray emitters (with marks “XX” or “XXX”).

While several of the X-ray sources had been already detected by the *Einstein Observatory* (with 2E designation), most of them, including Mayrit 750107, had been followed up with *ROSAT* by Wolk (1996; with [W96] designations), *XMM-Newton* by Franciosini et al. (2006; with [FPS2006] designation), and *Chandra* by Skinner et al. (2008). However, some strong X-ray sources and optical counterparts at the largest angular separations from the σ Orionis center, where most of X-ray studies have focused on, had escaped from previous *XMM-Newton* and *Chandra* observations (e.g. Mayrit 969077 had been identified only by the *Einstein Observatory*).

Of the 23 Mayrit stars, three are (multiple) OB-type systems and 15 have a fundamental spectroscopic feature of youth: Li I $\lambda 6707.8\text{\AA}$ in evident absorption. Some of them have also H α $\lambda 6562.8\text{\AA}$ in strong, asymmetric emission, which is an indication of accretion from a disk, or even have flux excesses at $3.8\text{--}8.0\mu\text{m}$ detected with *Spitzer* (marked with “class II” in Table 2; Hernández et al. 2007 also claimed that Mayrit 114305 and Mayrit 634052 have evolved and debris disks, respectively). The remaining five Mayrit stars without spectroscopic features of youth are strong X-ray sources with stellar spectral energy distributions in Franciosini et al. (2006) and colors and magnitudes consistent with membership in clus-

³Note the non-standard definition of χ^2 and the different nomenclature in Fuhrmeister & Schmitt (2003) for the same parameters: $\overline{CR} \equiv \mu$, $CR_i \equiv r_i$, $\delta CR_i \equiv e_i$. Besides, in their work, the number of events and of scans was identical ($N \equiv n$).

ter.

2.4. X-ray variability

Among the huge number of variability indicators that exist in the literature, we used a novel method based on the comparison of the measured χ^2 (Eq. 1) of our X-ray series and a large ensemble of Monte Carlo χ^2 s of simulated, non-variable, X-ray series. In short, we classified X-ray sources as variable if their χ^2 s are much larger than those of stable sources. Since the number of stable sources in the field of view was expected to be low (Feigelson & Montmerle 1999 hypothesized that all X-ray emitters, especially young stellar objects, are X-ray variable to some degree), we relied on simulating a large number of suitable light curves of “comparison stars”. As defined in Eq. 1, our χ^2 depends on the number of events, N , associated to each X-ray source, the mean net count rate, \overline{CR} , and the individual count rates and errors, CR_i and δCR_i . For a correct comparison, the simulated X-ray series must share identical parameters to the observed ones. Next, we describe how we computed these simulated X-ray series.

2.4.1. From \overline{CR} to N

The larger the mean net count rate of an X-ray source (\overline{CR}) is, the larger the number of associated events (N) is. This variation is illustrated in Fig. 4. Except for two Mayrit stars, all the X-ray sources *approximately* follow a sigmoid function defined as:

$$N(\overline{CR}) = \frac{A}{1 + \frac{B}{\overline{CR}^s}}, \quad (2)$$

where we assume $A = 150$, $B = 5 \cdot 10^4$, and $s = 5$. Variations of $\sim 10\%$ in these parameters still provide suitable fittings. The larger value of the exponent s makes the sigmoid function to “saturate” at a maximum value of A for a few tens counts per kilosecond ($N = 150$ for $\overline{CR} \gtrsim 20 \text{ ks}^{-1}$), but also to trace the steep raise of N at $\overline{CR} \sim 7 - 12 \text{ ks}^{-1}$. Besides, a sigmoid function like this one gives $N \approx 0$ for null \overline{CR} . The two outlier data points in Fig. 4 correspond to Mayrit 653170 ($N = 37$, $\overline{CR} = 14.235 \text{ ks}^{-1}$) and Mayrit 969077 ($N = 33$, $\overline{CR} = 27.955 \text{ ks}^{-1}$). Both of them displayed prominent flares among the 24 X-ray series, which affected the determination of the mean net count rate (see

below). The quiescent values \overline{CR} correspond to the number of associated events (and *vice versa*). Since we are interested in generating non-variable, simulated, X-ray series (i.e. flare-free series), we did not take into account these two outlier data points. We do not know whether the relatively low number of events for the mean net count rate in σ Ori AF-B is due to an observational (instrumental) bias.

2.4.2. From \overline{CR} to CR_i and δCR_i

We used the MATLAB function `poissrnd` to generate $N(\overline{CR})$ random numbers, CR_i , following a Poissonian distribution with parameter $\lambda = \overline{CR}$. There is an error, δCR_i , associated to each random value CR_i . In Fig. 5, we plot the δCR_i vs. CR_i diagram for the 1976 investigated *real* events, without attending to which X-ray source they correspond. The great majority of the 1995 Feb–Mar data points follow a $\delta CR \approx 0.8 CR^{1/2}$ relation. In contrast, the 1992 Sep data points, with a better accuracy, follow a $\delta CR_i \approx 0.3 CR_i^{1/2}$ relation. However, they represent about 1% of all considered points and their contribution to the computation of χ^2 is very small. Thus, we assumed that the 1995 Feb–Mar relation is right for all *simulated* data points, as a general rule. Numerically, each random value CR_i and its associated error satisfy the following expression:

$$\delta CR_i(CR_i) = 0.8 CR_i^{1/2}. \quad (3)$$

Each collection of pairs of values CR_i and δCR_i , $i = 1 \dots N$, represent a simulated X-ray series (temporal information is unnecessary). The factor 0.8 corresponds to an average observational efficiency of $\sim 71\%$ (X-ray light curves without gaps have efficiencies of 100%; “gaps” are observations that gave no counts for each source).

2.4.3. From \overline{CR} to χ^2

From Table 1, there are more X-ray sources with lower mean net count rates than with higher ones. The distribution of net count rates approximately follow a power law $n(\overline{CR}) \propto \overline{CR}^{-0.5}$ (this is roughly the bright end of the σ Orionis X-ray luminosity function). We generated 10^5 values of \overline{CR} following this distribution and with the restriction $\max(\overline{CR}) = 200 \text{ ks}^{-1}$. For each value

\overline{CR}_j , where $j = 1...10^5$, we computed N_j (Section 2.4.1) and $CR_{j,i}$ and $\delta CR_{j,i}$, where $i = 1...N_j$ (Section 2.4.2). Finally, with the previous values, we derived the parameters $\sigma_{CR,j}$, $\overline{\delta CR}_j$, and χ_j^2 (Eq. 1) for each simulated series j . Fig. 6 shows the subsequent χ_j^2 vs. \overline{CR}_j diagrams for the 10^5 simulated series and the 24 real series.

2.4.4. The variability criterion

We splitted the full interval of net count rates (from 4 to 200 ks^{-1}) of the simulated data into left panel in Fig. 6 in a number of bins, where we computed the value of χ^2 that leaves above it only 1 % of the data points. In other words, every data point above this χ^2 boundary has a probability $p_{\text{var}} > 99\%$ of being a true variable X-ray source. From larger to smaller average net count rates, the boundary is stable at $\chi^2 \approx 2.05$ from $\overline{CR} = 200$ down to 50 ks^{-1} , where it starts to increase softly up to $\chi^2 \approx 2.90$ at $\overline{CR} = 10 \text{ ks}^{-1}$. Then, there is a steep raise up to an approximate value of $\chi^2 = 6.5 \pm 0.5$ at $4\text{--}8 \text{ ks}^{-1}$ (the plateau value of the χ^2 boundary in the lowest energy interval is not as well constrained as in other intervals). Just for clarity, the χ^2 boundary is plotted only in right panel in Fig. 6.

3. Results

The average of the accurate data taken in 1992 Sep is consistent with the mean quiescent level in 1995 Feb–Mar for everyone of the 24 X-ray sources (i.e. there are no yearly variable sources from our HRI data only). However, there are six X-ray sources that clearly depart from the 1 % χ^2 boundary in Fig. 6 and have, therefore, probabilities $p_{\text{var}} \gg 99\%$ of being variables in scales of days. Of the six sources, five are stars and one is the galaxy 2E 1456. Besides, there are other four stars with $\overline{CR} = 10.2\text{--}11.3 \text{ ks}^{-1}$ that fall at the variability criterion boundary (three above, one below) and shall also be considered. Next, we discuss the variable and non-variable sources in detail.

3.1. Variable sources

3.1.1. Mayrit 653170: an X-ray flaring classical T Tauri star

Mayrit 653170 (RU Ori, Haro 5–15) is a long-time known classical T Tauri star. First discovered as a photometric variable in 1906 from Sonneberg (Kinnunen & Skiff 2002) and recovered by Haro & Moreno (1953) as a strong $H\alpha$ emitter, the star went almost unnoticed for nearly one century until Wolk (1996) found its X-ray emission. Mayrit 653170 has Li I in absorption (Caballero 2006; Sacco et al. 2008), He I $\lambda 10830 \text{ \AA}$ and $\text{P}\gamma$ $\lambda 10938 \text{ \AA}$ in emission (Gatti et al. 2008), a late-K or early-M spectral type, a radial velocity consistent with membership in the σ Orionis cluster (González-Hernández et al. 2008 and references above), and a spectral energy distribution typical of disk-host stars (Hernández et al. 2007).

The *ROSAT* quiescent level of Mayrit 653170 laid at $CR = 7 \pm 3 \text{ ks}^{-1}$. However, on 1995 Mar 7, the space mission detected five X-ray events with $CR = 59 \pm 5 \text{ ks}^{-1}$ (i.e. eight times above the quiescent level). The star recovered the quiescent level the following day, when three events with $CR < 6 \text{ ks}^{-1}$ were detected.

3.1.2. Mayrit 783254 and its violent long-lived flare

Mayrit 783254 (2E 1455, $M = 1.5 \pm 0.1 M_{\odot}$), although it is one of the brightest cluster stars in the optical (Caballero 2007a) and in X-rays (Franciosini et al. 2006), has been poorly investigated. Wolk (1996) determined a K0 spectral type and found both $H\alpha$ and Li I in absorption. It has no mid-infrared flux excess (Luhman et al. 2008). Mayrit 783254 displayed a long-lived X-ray flare that lasted at least three days during the *ROSAT* observations. The flux increase, of a factor six, was smaller than for Mayrit 653170, but still very clear in the X-ray light curve in top panel in Fig. 13. Five events at $CR = 113 \pm 11 \text{ ks}^{-1}$ on 1995 Mar 11 marked the maximum of the flare. At this moment, Mayrit 783254 was the second brightest source in the cluster, with only 11 % less soft X-ray flux than σ Ori AF-B.

The increasing factor and shape of the Mayrit 783254 flare were similar to those observed in some stars of the Taurus star-forming complex (Gia-

rdino et al. 2006; Franciosini et al. 2007). However, to the contrary of the Taurus stars, whose rise phases last less than one day, here we observe that the net count rate increased during a minimum of three days. We suspect that the rapid decrease in the count rate after the maximum is due to the occultation of the flaring region due to the star rotation, and that the flare could have lasted for more than five or six days. Such long-duration X-ray flaring events have been observed in some stars of Orion (e.g. Favata et al. 2005). In those cases, the events were associated with long structures (loops) anchored at the inner part of disks. However, a similar event has also been studied by Crespo-Chacón et al. (2008) in a star of the TW Hydra association, in which the long-duration rise phase is attributed to the propagation of the energy of the first flare along a very large arcade (e.g. Poletto et al. 1988). In any case, we have no temporal and spectral resolution enough to study the case of Mayrit 783254 in detail and we cannot distinguish between both scenarios (a long loop vs. an arcade).

3.1.3. Mayrit 969077: another flare star

Mayrit 969077 (2E 1487) first appeared in the *Einstein* catalogs by Harris et al. (1994) and Moran et al. (1996). There is no spectroscopic information available⁴ and it also lacks a disk (Luhman et al. 2008). It fell out of the *XMM-Newton* observations by Franciosini et al. (2006) and, consequently, of the narrower *Chandra* observations by Skinner et al. (2008). The quiescent X-ray level of Mayrit 969077 seems to be very low (at $CR = 10 \text{ ks}^{-1}$ or lower), that made the star to be undetected during the first half of the 1995 Feb–Mar run. However, since Mar 17 to Mar 23, Mayrit 969077 produced a strong flare with a maximum of $CR = 59 \pm 7 \text{ ks}^{-1}$ on Mar 20. The shape of the ~ 6 d-long flare was quite symmetric. In this case, the lack of a disk suggests that the event might be due to an overposition of flares in an arcade. Large high-energy flares with durations of ~ 3 –6 d, although rare, have been detected in neighbouring stars with a “vigorous rotationally driven magnetic dynamo”, such

as the RS CVn-type stars UX Ari, σ Gem, and V711 Tau observed with the *Extreme Ultraviolet Explorer* (*EUVE*) mission (Osten & Brown 1999; Sanz-Forcada et al. 2003). RS CVn-type stars are close binaries ($P_{\text{orb}} \sim 1$ –14 d), so we cannot rule out a binary hypothesis for Mayrit 969077.

3.1.4. The bright star Mayrit 863116

Mayrit 863116 (RX J0539.6–0242) is a G5–K0-type, weak-lined T Tauri star with cosmic lithium abundance, $H\alpha$ filled in with emission, radial velocity consistent with membership in σ Orionis, and a broad cross-correlation function (probably due to its high rotational velocity of $v \sin i = 150 \text{ km s}^{-1}$ or to unresolved binarity; Alcalá et al. 1996, 2000). Although it is the 19th brightest σ Orionis star in the optical, it moves to the ninth position in the near-infrared (Caballero 2008b). This is due to its very red $V_T - K_s$ color for its magnitude, of $2.25 \pm 0.05 \text{ mag}$, which may be indicative of the presence of a surrounding disk (Caballero 2007a). However, Hernández et al. (2007) failed to detect any flux excess with *Spitzer* IRAC (4.5–8.0 μm) and MIPS (24 μm).

The X-ray series of Mayrit 863116 shown in top panel of Fig. 14 displayed a flare on 1995 Mar 25 with a peak of $CR = 81 \pm 7 \text{ ks}^{-1}$, at about four times above the approximate quiescent level. This level seems to be variable in its turn, with short time scale variations from 10 to 30 ks^{-1} around the approximate average value of 20 ks^{-1} .

3.1.5. The faint star Mayrit 156353

Mayrit 156353 ([SWW2004] 36) is a photometric cluster member candidate detected by Sherry et al. (2004) with a moderate X-ray emission measured by Franciosini et al. (2006). The last authors estimated an M1 spectral type from optical/near-infrared colors and empirical color-magnitude relations. They also classified Mayrit 156353 as a cluster member showing significant variability not clearly attributable to flares. It is the faintest star in Table 2 at all wavelengths and is located relatively close to the cluster center ($\rho \sim 2.6 \text{ arcmin}$). On 1995 Mar 8, the X-ray flux of Mayrit 156353 peaked with three events of $CR = 24 \pm 3 \text{ ks}^{-1}$, about five times above the low quiescent level at $CR \sim 5 \text{ ks}^{-1}$.

⁴Due to a typographical error, Caballero (2008b) incorrectly tabulated Mayrit 969077 as having $H\alpha$ in emission and Li I in absorption.

3.1.6. The galaxy 2E 1456

The abnormally blue $i - J$ and red $J - K_s$ colors, strong X-ray emission, and extended point-spread-function of the *Einstein* source 2E 1456 led Caballero (2008b) to classify it as a galaxy in the background of σ Orionis. Afterwards, López-Santiago & Caballero (2008) investigated its spectral energy distribution from 0.3 to 7.5 keV using *XMM-Newton* data (source NX 32) and confirmed its extragalactic nature. The net count rates of 2E 1456 in our *ROSAT* data varied from 20 to 60 ks⁻¹, approximately, with time scales of variations of a few days. Unfortunately, the X-ray series of 2E 1456 obtained with *XMM-Newton* by Franciosini et al. (2006) and López-Santiago & Caballero (2008) could not be searched for short-scale variability due to several reasons.

The confusion of extragalactic sources with σ Orionis member candidates is not rare (Caballero et al. 2008), but 2E 1456 being the second brightest X-ray source in the area after σ Ori AF-B turns out remarkable, if not singular. 2E 1456 probably harbours an active galactic nucleus (AGN – Rees 1984; Elvis et al. 1994). The power-law photon index derived by López-Santiago & Caballero (2008), $\Gamma = 1.82$, is consistent with 2E 1456 being a Seyfert galaxy with a supermassive black hole (e.g. Nandra & Pounds 1994). Since the highest energy photons in these galaxies are believed to be created by inverse Compton scattering by a high temperature corona near the compact black hole, the observed X-ray variability in time scales of a few days is not difficult to explain.

3.1.7. Four possible variable stars with $p_{\text{var}} \sim 99\%$

From Fig. 6, there are four stars with $CR = 10.2\text{--}11.3\text{ks}^{-1}$ and relatively large χ^2 values corresponding to probabilities of variability at the 1% χ^2 boundary. Two of them, both with $p_{\text{var}} \gtrsim 99\%$, are chemically peculiar early-type stars: Mayrit 42062 (σ Ori E; B2Vp) and Mayrit 306125 (HD 37525; B5Vp). Their variable X-ray emission would be difficult to explain if they were single (Skinner et al. 2008), especially in the case of the flare of Mayrit 42062. Previously, strong X-ray flares in Mayrit 42062 had been reported by Groote & Schmitt (2004; using these

very same HRI observations) and Sanz-Forcada et al. (2004). Such flares are typical in young late-type stars, but virtually missing in early-type stars like Mayrit 42062. Besides, Skinner et al. (2008) detected no large flares on it, although they saw a possible sinusoidal variation with a period consistent with the stellar rotation period $P \sim 1.19\text{d}$. After decades of unfruitful searches (Landstreet & Borra 1978; Groote & Hunger 1982; Drake et al. 1994; Townsend et al. 2005 and references therein), Bouy et al. (2009) finally discovered the low-mass companion at only $\rho \approx 0.330\text{arcsec}$ to Mayrit 42062. This late-type companion is likely the origin of the detected flares (it is also plausible that the B2Vp star itself is the only source of the X-ray emission, including the variability – ud-Doula et al. 2006; Townsend et al. 2007). Likewise, Mayrit 306125 is another binary: Caballero (2006) resolved a companion of the primary about 0.5 mag fainter at $\rho = 0.47 \pm 0.04\text{arcsec}$ (see also Caballero 2005). However, from the magnitude difference in this case, the companion Mayrit 306125 B must be a late B- or an early A-type star. The combined X-ray lightcurve of the binary system does not show apparent flare events, but a soft variation from 5 to 17 ks⁻¹ in time scales of tens of days. Variable colliding wind shocks of the two components may play an important rôle in the X-ray emission of the system.

The other two possible variable stars are Mayrit 203039 ([W96] 4771–1049; $p_{\text{var}} \gtrsim 99\%$) and Mayrit 114305 ([W96] 4771–1147 AB; $p_{\text{var}} \lesssim 99\%$). Skinner et al. (2008) also measured variability probabilities larger than 99 and 97%, respectively, from *Chandra* data. On the one hand, Mayrit 203039 has a K5 spectral type, Li I in absorption, and H α in chromospheric emission (Wolk 1996). A short-duration flare, that persisted for no less than the last 4 h of their observations, was discovered by Franciosini et al. (2006). The time series from our data in middle panel of Fig. 10 does not evidence apparent flare events in Mayrit 203039, but quasi-periodic variations from 5 to 22 ks⁻¹ in time scales of tens of days. Lower-amplitude, higher-frequency variations could be superimposed to the main trend. On the other hand, Mayrit 114305 displays quite similar properties, except for an earlier spectral type (K0), a spectroscopic binary status (Wolk

1996), and a possible evolved disk (Hernández et al. 2007). Given its proximity to the cluster center ($\rho = 1.9$ arcmin), it has been investigated in other X-ray surveys in σ Orionis (Sanz-Forcada et al. 2004; Franciosini et al. 2006; Caballero 2007b). The time series of Mayrit 114305, shown in top panel of Fig. 9, displayed two clear flares on 1995 Mar 9 and 19 with peaks of $CR = 26 \pm 5$ and $25 \pm 4 \text{ ks}^{-1}$, respectively (five X-ray events each).

3.2. Non-variable stars

In our data, there are two stars with large mean net count rates and low values of χ^2 and are, therefore, suitable examples of non-variable X-ray stars. They are σ Ori AF-B and Mayrit 789281 (2E 1454; but see Section 4). The absence of mid-term variability in the massive triple system confirms previous results by Groote & Schmitt (1994; see also Skinner et al. 2008 for a detailed discussion on the origin of its X-ray emission). However, Mayrit 789281 is a late-G or early-K T Tauri star with cosmic lithium abundance and H α in broad emission (Caballero 2006; González-Hernández et al. 2008). Its radial velocity matches the average one of the “Group 1” of young stars that contaminate the σ Orionis cluster and belong to an overlapping not-so-young stellar population in the Orion Belt (Jeffries et al. 2006). The X-ray time series of Mayrit 789281 maintained very stable at $CR = 19 \pm 4 \text{ ks}^{-1}$, with no outlier data points.

The remaining 12 stars are below the boundary of $p_{\text{var}} = 99\%$ and are classified in this work as non-variable stars with our conservative classification criterion. Nevertheless, the 12 of them have $\overline{CR} < 10 \text{ ks}^{-1}$, where the boundary of $p_{\text{var}} = 99\%$ was not well constrained. Furthermore, the X-ray time series of a few stars, like Mayrit 105249 ([W96] rJ053838–0236) and Mayrit 344337 ([W96] 4771–1097), display flare-like events and have values of χ^2 close to the boundary of $p_{\text{var}} = 99\%$ (the two of them were classified as cluster members showing significant variability not clearly attributable to flares by Franciosini et al. 2006; Mayrit 105249 did show flaring activity in Skinner et al. 2008 data). Instead of being suspicious of the actual variability of the faint flare star Mayrit 156353 (also with $\overline{CR} < 10 \text{ ks}^{-1}$; Section 3.1.5), we are suspicious of the non-variability of some of our 12 “non-variable”

stars. In any case, we prefer being cautious and claiming the variability and possible variability from our data of only the other nine stars (and one galaxy) in Section 3.1.

4. Discussion

Using an *XMM-Newton* dataset, Sanz-Forcada et al. (2004) and Franciosini et al. (2006) reported strong flare events in 12 σ Orionis stars. Ten of them were too faint for our HRI *ROSAT*; the other two bright X-ray sources were Mayrit 203039 and Mayrit 42062 (classified in our work as possible variables; Section 3.1.7). Another five stars in Franciosini et al. (2006) showed significant variability not clearly attributable to flares. Of them, four have been investigated here and only one, Mayrit 207358, had no hint of variability from our χ^2 analysis. Besides, of the nine X-ray HRI stars in common with Skinner et al. (2008), four had variability probabilities larger than 97% in their work. Three of them are among the four possible variable stars with $p_{\text{var}} \sim 99\%$ (Section 3.1.7) and the remaining one is Mayrit 105249, which we classified as a questionable non-variable star. All these facts indicate that our “possible variable stars” likely vary.

The variability criterion that we used in Section 3, although it was computed through an apparently complicated method, gives the same results as if we had searched for flares in the light curves with the naked eye. We also performed single sample goodness-of-fit hypothesis Kolmogorov-Smirnov tests on the HRI time series by assuming hypothetical Poissonian cumulative distributions functions of mean $\lambda = \overline{CR}$ (we used the MATLAB functions `poisscdf` and `kstest`). In last column in Table 1, we provide the corresponding Kolmogorov-Smirnov p -values (a source with a p -value $p_{K-S}(\overline{\lambda})$ has a probability $1 - p_{K-S}(\overline{\lambda})$ of being variable). All except five sources do not reject the null hypothesis at significance level $\alpha \equiv p_{K-S}(\overline{\lambda}) = 10^{-7}$. The five of them are among the six variable sources in Section 3.1. The sixth variable there, the faint star Mayrit 156353, has a p -value less than $2 \cdot 10^{-4}$. Another six stars have p -values below the $5 \cdot 10^{-3}$ threshold (with K-S variability probabilities larger than 99.5%). All of them except one are discussed here as probable variables or questionable

non-variables. The only inconsistency between our χ^2 and Kolmogorov-Smirnov analyses is the apparently stable young star Mayrit 789281, which has $p_{K-S}(\bar{\lambda}) \approx 1.3 \cdot 10^{-4}$. Another variability criteria, such as maximum likelihood block algorithm, would have led us to comparable outcomes if they were to be performed (Wolk et al. 2005; Stelzer et al. 2007; Albacete Colombo et al. 2007b).

The existence of nine HRI variable stars [five if not accounting for the possible variables in Section 3.1.7] among a list of 23 stars leads to a frequency of mid-term X-ray variability of 39% [22% if not accounting for the possible variables]⁵. Except in two cases (the possible variable stars Mayrit 306125 and Mayrit 203039), the origin of the X-ray variability is the presence of flaring events.

Five [seven] of the six [ten] sources with $p_{\text{var}} \gg 99\%$ [$p_{\text{var}} \gtrsim 99\%$] (including the galaxy) are among the seven [eleven] brightest X-ray sources. This is an evidence of a bias towards the non-detection of variability among the faintest sources. Therefore, the actual frequency of mid-term X-ray variability in σ Orionis must be larger than 39% [22%]. Observational selection and statistical effects in the determination of X-ray variability have been discussed in detail by, e.g., Stelzer et al. (2000; with *ROSAT*) and Albacete Colombo et al. (2007a; with *Chandra*).

In the literature, there have been numerous studies of X-ray variability and flaring activity of stars with *ROSAT*: M- and F7–K2-type dwarfs in the solar neighbourhood (Marino et al. 2000, 2002), stars in clusters significantly older than σ Orionis (such as α Persei, $\tau \sim 90$ Ma; Prosser et al. 1996), or stars in the Taurus-Auriga-Perseus sky region (with Taurus star forming region, Pleiades, and Hyades-like ages; Stelzer et al. 2000). With the arrival of *XMM-Newton* and *Chandra*, larger samples of stars in young clusters are observed (Preibisch & Zinnecker 2002 in IC 348; Gagné et al. 2004 in ρ Ophiuchi; Marino et al. 2005 in IC 2391). The most comprehensive searches for X-ray variability have been carried out in the Orion Nebula Cluster with *Chandra* by Feigelson et al. (2002), Favata et al. (2005),

and Wolk et al. (2005). Reported frequencies of X-ray variabilities range between $<5\%$ in the field to $\sim 46\%$ in IC 2391 ($\tau \sim 40$ Ma). Our measured X-ray variability of 39% [22%] lays within this range. However, due to the different spectral response of the X-ray missions, stellar ages, and depth, length, and temporal resolution of observations, our derived frequency of X-ray variability is not *directly* comparable to these determinations. We insist that the data and analysis presented in this paper are sensitive to relatively high amplitude variability on timescales in excess of a day, but insensitive to other types of variability. Nevertheless, our work complements satisfactorily previous X-ray variability studies in young stars in the σ Orionis cluster, especially those by Franciosini et al. (2006) and Skinner et al. (2008). Although our HRI data prevented us from detecting low amplitude variability and in scales shorter than a few hours, *ROSAT* archival data are to date the only way to investigate X-ray variations in scales of days.

Likewise, we could not perform any study of the flare energy distribution due to the obvious limitations of the HRI *ROSAT* observation in terms of time coverage (one observation of about $2.2 \text{ ks} \approx 0.025 \text{ d}$ every day), spectral coverage (0.1–2.4 keV), and spectral resolution (there is no defined bands in the 1RXH catalogue). Results on this topic in other star forming regions investigated with *Chandra* and *XMM-Newton* have been presented by other authors, such as Albacete Colombo et al. (2007b) in the the Cyg OB2 association and Orion Nebula Cluster and Stelzer et al. (2007) in Taurus.

Taking into account the compiled spectrophotometric information and the *iJHK_s* magnitudes in the Mayrit catalog (Caballero 2008b), we looked for particular features of the X-ray variable stars, especially the presence of (accretion) circumstellar disks. There is a tendency of disk-host classical T Tauri stars to be less X-ray luminous than disk-free young stars (Neuhäuser et al. 1995 in Taurus; Franciosini et al. 2006 and Caballero 2007b in σ Orionis). More importantly, disk-free stars, which rotate faster than stars magnetically locked by disks, are more X-ray active (Güdel 2004; Preibisch et al. 2005). The enhancement of the activity by fast stellar rotation is also applied to σ Orionis. While the frequency

⁵Because of the two different ways of computing the frequency of X-ray variability, we do not give error bars. If computed, it should be as in Burgasser et al. (2003).

of disks in the cluster at almost all mass intervals lies at about 50 % (Caballero 2007a and references therein; Sacco et al. 2008; Luhman et al. 2008), only one (the classical T Tauri star Mayrit 653170 in Section 3.1.1) of the nine [five] stars with $p_{\text{var}} \gtrsim 99\%$ [$p_{\text{var}} \gg 99\%$] is a class II object with mid-infrared flux excess due to a disk. In other words, the frequency of mid-term X-ray variable stars with disks in our sample is 11 % [20 %]. If both disk-free and disk-host σ Orionis stars had the same X-ray properties (i.e. the same rotational velocity and subsequent activity), we would expect four or five [two or three] ($\sim 50\%$) class II objects with mid-term variability instead of only one. Apart from the disk-host star Mayrit 653170, there is no trend between X-ray variability and optical/near-infrared colors or H α emission. A detailed study of the frequency of flares and X-ray properties in stars with and without disk in a large sample of members of the σ Orionis cluster observed with HRC-I onboard *Chandra* is being done by the authors and will be presented in a forthcoming paper.

5. Summary

Using Virtual Observatory tools and HRI *ROSAT* public data, we have investigated the X-ray variability in scale of days of 23 stars in the young σ Orionis cluster. Catalogued data covered more than 30 d in 1995 Feb–Mar. The time series of five stars displayed clear flare events (with probabilities $p_{\text{var}} \gg 99\%$ of being variable); several of these flares were violent and lasted for up to six days. Another four stars seemed to be also variable in scales of days. All the flaring activity identifications are new except for Mayrit 203039 (a weak-lined T Tauri star) and Mayrit 42062 (σ Ori E and its close faint companion), for which we confirm the display of flares. Since our data are insensitive to low-amplitude variations or with time scales shorter than one day, the actual frequency of X-ray variables among σ Orionis is larger than 39 %. Classical T Tauri stars with disks are less X-ray variable (or, alternatively, less X-ray luminous) than disk-free young stars, which presumably rotate faster. Besides, we have identified an AGN-host galaxy with an intense, variable X-ray emission.

We are grateful to the anonymous referee, J. F. Albacete Colombo, and J. Sanz-Forcada for helpful discussion and advice. Financial support was provided by the Universidad Complutense de Madrid, the Comunidad Autónoma de Madrid, the Spanish Ministerio Educación y Ciencia, and the European Social Fund under grants: AyA2005-02750, AyA2005-04286, AyA2005-24102-E, AyA2008-06423-C03-03, AyA2008-00695, PRICIT S-0505/ESP-0237, and CSD2006-0070. This research has made use of the SIMBAD, operated at Centre de Données astronomiques de Strasbourg, France, and the NASA’s Astrophysics Data System.

REFERENCES

- Albacete Colombo, J. F., Flaccomio, E., Micela, G., Sciortino, S., Damiani, F. 2007a, *A&A*, 464, 211
- Albacete Colombo, J. F., Caramazza, M., Flaccomio, E., Micela, G., Sciortino, S. 2007b, *A&A*, 474, 495
- Alcalá, J. M., Terranegra, L., Wichmann, R. et al. 1996, *A&AS*, 119, 7
- Alcalá, J. M., Covino, E., Torres, G. et al. 2000, *A&A*, 353, 186
- Berghöfer, T. W. & Schmitt, J. H. M. M. 1994, *A&A*, 290, 435
- Bonnarel, F., Fernique, P., Bienaymé, O. et al. 2000, *A&AS*, 143, 33
- Bouy, H., Huélamo, N., Martín, E. L. et al. 2009, *A&A*, 493, 931
- Burgasser, A. J., Kirkpatrick, J. D., Reid, I. N. et al. 2003, *ApJ*, 586, 512
- Caballero, J. A. 2005, *AN*, 326, 1007
- Caballero, J. A. 2006, Ph.D. thesis, Universidad de La Laguna, Spain (arXiv:0810.2033)
- Caballero, J. A. 2007a, *A&A*, 466, 917
- Caballero, J. A. 2007b, *AN*, 328, 917
- Caballero, J. A. 2008a, *MNRAS*, 383, 375
- Caballero, J. A. 2008b, *A&A*, 478, 667

- Caballero, J. A. 2009, *Multi-wavelength Astronomy and Virtual Observatory Workshop*, European Space Astronomy Centre, Villafranca del Castillo, Madrid, Spain, 1–3 Dec 2008, in press (arXiv:0901.2566)
- Caballero, J. A., Valdivielso, J., Martín, E. L. et al. 2008, *A&A*, 491, 515
- Crespo-Chacón, I., López-Santiago, J., Reale, F., Micela, G. 2008, 15th Cambridge Workshop on Cool Stars, Stellar Systems, and the Sun ASP Conference Series, proceedings of the conference held 21-25 July, 2008, at the University of St. Andrews, St. Andrews, Scotland, UK. Ed. E. Stempels. Poster #G3
- ud-Doula, A., Townsend, R. H. D., Owocki, S. P. 2006, *ApJ*, 640, L191
- Drake, S. A., Linsky, J. L., Schmitt, J. H. M. M., Rosso, C. 1994, *ApJ*, 420, 387
- Elvis, M., Wilkes, B. J., McDowell, J. C. et al. 1994, *ApJS*, 95, 1
- Favata, F., Flaccomio, E., Reale, F., et al. 2005, *ApJS*, 160, 469
- Feigelson, E. D. & Montmerle, T. 1999, *ARA&A*, 37, 363
- Franciosini, E., Pallavicini, R., Sanz-Forcada, J. 2006, *A&A*, 446, 501
- Franciosini, E., Pillitteri, I., Stelzer, B., et al. 2007, *A&A*, 468, 485
- Fuhrmeister, B. & Schmitt, J. H. M. M. 2003, *A&A*, 403, 247
- Gatti, T., Natta, A., Randich, S., Testi, L., Sacco, G. 2008, *A&A*, 481, 423
- Giardino, G., Favata, F., Silva, B., et al. 2006, *A&A*, 453, 241
- González-Hernández, J. I., Caballero, J. A., Rebolo, R. et al. 2008, *A&A*, 490, 1135
- Groote, D. & Hunger, K. 1982, *A&A*, 116, 64
- Groote, D. & Schmitt, J. H. M. M. 2004, *A&A*, 418, 235
- Güdel, M. 2004, *A&ARv*, 12, 71
- Haro, G. & Moreno, A. 1953, *Bol. Obs. Tonantz. Tacub.*, 1, part no. 7, 11
- Harris D.E., Forman W, Gioia I.M. et al. 1994, *VizieR On-line Data Catalog: IX/13*. Originally published in: *Einstein* Observatory catalog of IPC X-ray sources, SAO HEAD CD-ROM Series I (Einstein), Nos. 18–36
- Hernández, J., Hartmann, L., Megeath, T. et al. 2007, *ApJ*, 662, 1067
- Jeffries, R. D., Maxted, P. F. L., Oliveira, J. M., Naylor, T. 2006, *MNRAS*, 371, L6
- Kinnunen, T. & Skiff, B. A. 2002, *VizieR On-line Data Catalog: IV/23*. Originally published in: Kinnunen, T. & Skiff, B. A. 2000, *IBVS*, 4861, 1
- Landstreet, J. D. & Borra, E. F. 1978, *ApJ*, 224, L5
- López-Santiago, J. & Caballero, J. A. 2008, *A&A*, 491, 961
- Luhman, K. L., Hernández, J., Downes, J. J., Hartmann, L., Briceño, C. 2008, *ApJ*, 688, 362
- Marino, A., Micela, G., Peres, G. 2000, *A&A*, 353, 177
- Marino, A., Micela, G., Peres, G., Sciortino, S. 2002, *A&A*, 383, 210
- Marino, A., Micela, G., Peres, G., Pillitteri, I., Sciortino, S. 2005, *A&A*, 430, 287
- Moran, E. C., Helfand, D. J., Becker, R. H., White, R. L. 2006, *ApJ*, 461, 127
- Nandra, K. & Pounds, K. A. 1994, *MNRAS*, 268, 405
- Neuhäuser, R., Sterzik, M. F., Schmitt, J. H. M. M., Wichmann, R., Krautter, J. 1995, *A&A*, 297, 391
- Osten, R. A. & Brown, A. 1999, *ApJ*, 515, 746
- Poletto, G., Pallavicini, R., Kopp, R. A. 1988, *A&A*, 201, 93
- Preibisch, T., Kim, Y.-C., Favata, F. et al. 2005, *ApJS*, 160, 410
- Rees, M. J. 1984, *ARA&A*, 22, 471

- ROSAT* Consortium (*) 2000, VizieR On-line Data Catalog: IX/28A. Originally published in: ROSAT NEWS No. 71 (*: Max-Planck-Institut fuer extraterrestrische Physik, Goddard Space Flight Center, Smithsonian Astrophysical Observatory Leicester University, Astrophysikalisches Institut Potsdam)
- Sacco, G. G., Franciosini, E., Randich, S., Pallavicini, R. 2008, *A&A*, 488, 167
- Sanz-Forcada, J., Brickhouse, N. S., Dupree, A. K. 2002, *ApJ*, 570, 799
- Sanz-Forcada, J., Franciosini, E., Pallavicini, R. 2004, *A&A*, 421, 715
- Sherry, W. H., Walter, F. M., Wolk, S. J. 2004, *AJ*, 128, 2316
- Sherry, W. H., Walter, F. M., Wolk, S. J., Adams, N. R. 2008, *AJ*, 135, 1616
- Skinner, S. L., Sokal, K. R., Cohen, D. H. et al. 2008, *ApJ*, 683, 796
- Stelzer, B., Neuhauser, R., Hambaryan, V. 2000, *A&A*, 356, 949
- Stelzer, B., Flaccomio, E., Briggs, K. et al. 2007, *A&A*, 468, 463
- Townsend, R. H. D., Owocki, S. P., Groote, D. 2005, 630, L81
- Townsend, R. H. D., Owocki, S. P., ud-Doula, A. 2007, *MNRAS*, 382, 139
- Walter, F. M., Sherry, W. H., Wolk, S. J., Adams, N. R. 2008, *Handbook of Star Forming Regions, Volume I: The Northern Sky ASP Monograph Publications*, Vol. 4. Edited by Bo Reipurth, p. 732
- Watson, M. G., Pye, J. P., Denby, M. et al. 2003, *AN*, 324, 89
- Watson, M. G., Schröder, A. C., Fyfe, D. et al. 2009, *A&A*, 493, 339
- Wolk, S. J. 1996, Ph.D. thesis, State University New York at Stony Brook, USA

TABLE 1
BRIGHT *ROSAT* SOURCES IN σ ORIONIS: OUR X-RAY PARAMETERS

Name	$\bar{\alpha}$ (J2000)	$\bar{\delta}$ (J2000)	σ_{α} [arcsec]	σ_{δ} [arcsec]	N	\overline{CR} [ks $^{-1}$]	σ_{CR} [ks $^{-1}$]	$\overline{\delta CR}$ [ks $^{-1}$]	χ^2	Var.	p_{K-S} (λ)
Mayrit AB	084.686413	-02.599601	1.4460	1.6507	127	127.61	8.2144	8.4512	1.0972	No	0.30
Mayrit 42062	084.696596	-02.594071	1.7106	2.0294	75	10.908	5.3903	2.4067	3.2179	Yes?	$1.5 \cdot 10^{-4}$
Mayrit 105249	084.658954	-02.610452	2.6008	2.2433	67	7.6745	5.4678	1.9472	5.8211	No:	$1.7 \cdot 10^{-5}$
Mayrit 114305	084.659967	-02.581494	2.3823	2.8311	145	12.627	4.5136	2.5663	2.4952	No?	$1.4 \cdot 10^{-4}$
Mayrit 156353	084.681297	-02.556549	1.4855	2.3738	37	7.0708	5.4232	1.8357	10.309	Yes	$1.7 \cdot 10^{-4}$
Mayrit 157155	084.704907	-02.639707	1.9022	1.9348	28	5.5457	1.3996	1.7400	0.8330	No	0.64
Mayrit 180277	084.636298	-02.593567	2.8343	2.9797	64	6.1658	2.7547	1.7486	3.1900	No	0.063
Mayrit 203039	084.722404	-02.555867	2.3429	2.4370	127	11.259	4.2434	2.4978	2.8527	Yes?	0.0011
Mayrit 207358	084.684171	-02.542337	2.2816	3.7694	101	7.8854	2.4518	2.0580	1.7690	No	0.12
Mayrit 260182	084.683889	-02.672494	2.2552	2.1461	36	7.2283	5.4087	1.9650	3.8026	No	$8.8 \cdot 10^{-5}$
Mayrit 285331	084.647531	-02.530589	2.2976	1.7840	36	6.9514	3.4081	1.9000	2.9707	No	0.29
Mayrit 306125	084.756245	-02.649166	2.0980	3.2594	120	10.207	3.4418	2.3645	3.5731	Yes?	$2.0 \cdot 10^{-4}$
Mayrit 344337	084.649288	-02.511315	2.1160	2.7610	33	6.2621	3.8114	1.7788	5.5412	No:	0.0044
Mayrit 528005	084.700105	-02.452731	2.5920	2.3517	58	8.2898	2.9667	2.3005	3.1352	No	0.024
Mayrit 615296	084.531778	-02.524775	2.9341	2.6624	96	9.2787	2.3336	2.5375	1.3998	No	0.077
Mayrit 634052	084.825398	-02.490467	3.5232	4.0022	42	7.9033	3.1513	2.4155	3.5873	No	0.12
Mayrit 653170	084.716724	-02.779516	3.5521	2.1357	37	14.235	18.075	2.4011	28.487	Yes	$8.9 \cdot 10^{-18}$
Mayrit 750107	084.886696	-02.662064	3.7316	3.8277	28	8.1939	3.4150	2.5711	3.7112	No	0.018
Mayrit 783254	084.475637	-02.657996	3.8509	2.7251	159	23.902	17.473	4.2384	5.1667	Yes	$8.5 \cdot 10^{-19}$
Mayrit 789281	084.469905	-02.559010	3.9973	3.8648	147	18.939	3.9355	3.8728	1.0496	No	$1.3 \cdot 10^{-4}$
Mayrit 822170	084.725095	-02.825619	3.4521	3.7930	43	9.0223	3.8657	2.6023	3.1078	No	0.032
Mayrit 863116	084.902644	-02.704998	3.3539	3.6062	144	22.266	12.898	4.0868	5.2504	Yes	$1.2 \cdot 10^{-12}$
Mayrit 969077	084.949897	-02.539979	4.6934	4.8872	33	27.955	16.276	4.6606	18.825	Yes	$9.1 \cdot 10^{-8}$
2E 1456	084.483910	-02.753679	2.7119	2.9404	163	38.294	9.5044	5.4239	3.8583	Yes	$1.6 \cdot 10^{-9}$

TABLE 2
BRIGHT *ROSAT* SOURCES IN σ ORIONIS: OPTICAL COUNTERPARTS

Name	Alternative name	α (J2000)	δ (J2000)	J [mag]	Remarks
Mayrit AB	σ Ori A+B+F+IRS1	084.686518	-02.600047	4.020 \pm 0.010	OB, mIR
Mayrit 42062	σ Ori E (a+b)	084.696659	-02.594594	6.974 \pm 0.026	OB
Mayrit 105249	[W96] rJ053838-0236	084.659273	-02.610675	11.158 \pm 0.026	Li I, H α
Mayrit 114305	[W96] 4771-1147 AB	084.660359	-02.581950	9.097 \pm 0.027	Li I, H α
Mayrit 156353	[SWW2004] 36	084.681473	-02.557045	11.716 \pm 0.028	XX ([FPS2006] 76)
Mayrit 157155	[W96] rJ053849-0238	084.704888	-02.639512	11.389 \pm 0.023	Li I, H α
Mayrit 180277	[W96] rJ053832-0235b	084.636844	-02.594223	11.544 \pm 0.027	XXX ([FPS2006] 49)
Mayrit 203039	[W96] 4771-1049	084.722390	-02.556384	10.607 \pm 0.026	Li I, H α
Mayrit 207358	[W96] 4771-1055	084.684345	-02.542674	10.877 \pm 0.027	Li I
Mayrit 260182	[W96] 4771-1051	084.684299	-02.672143	11.363 \pm 0.026	Li I, H α , class II
Mayrit 285331	[W96] rJ053835-0231	084.647775	-02.531016	11.360 \pm 0.026	XX ([FPS2006] 60)
Mayrit 306125	HD 37525 AB	084.756235	-02.649011	8.131 \pm 0.030	OB
Mayrit 344337	[W96] 4771-1097	084.649467	-02.512033	11.245 \pm 0.026	Li I, H α
Mayrit 528005	[W96] 4771-899 AB	084.700149	-02.453943	10.156 \pm 0.023	Li I, H α , class II
Mayrit 615296	2E 1459	084.532698	-02.525389	10.566 \pm 0.027	Li I, H α
Mayrit 634052	[W96] 4771-0598	084.825298	-02.491239	10.721 \pm 0.027	XX ([FPS2006] 156)
Mayrit 653170	RU Ori	084.716695	-02.778798	11.518 \pm 0.026	Li I, H α , class II
Mayrit 750107	[W96] rJ053932-0239	084.885707	-02.662225	10.820 \pm 0.024	Li I
Mayrit 783254	2E 1455	084.476687	-02.658291	9.255 \pm 0.020	XXX ([FPS2006] 3)
Mayrit 789281	2E 1454	084.470982	-02.559558	9.991 \pm 0.027	Li I, H α
Mayrit 822170	RX J0538.9-0249	084.725444	-02.824937	10.829 \pm 0.026	Li I, H α
Mayrit 863116	RX J0539.6-0242	084.902263	-02.704768	8.462 \pm 0.027	Li I, H α
Mayrit 969077	2E 1487	084.949336	-02.540242	10.969 \pm 0.026	Li I, H α
2E 1456	...	084.484608	-02.753637	15.398 \pm 0.073	Galaxy

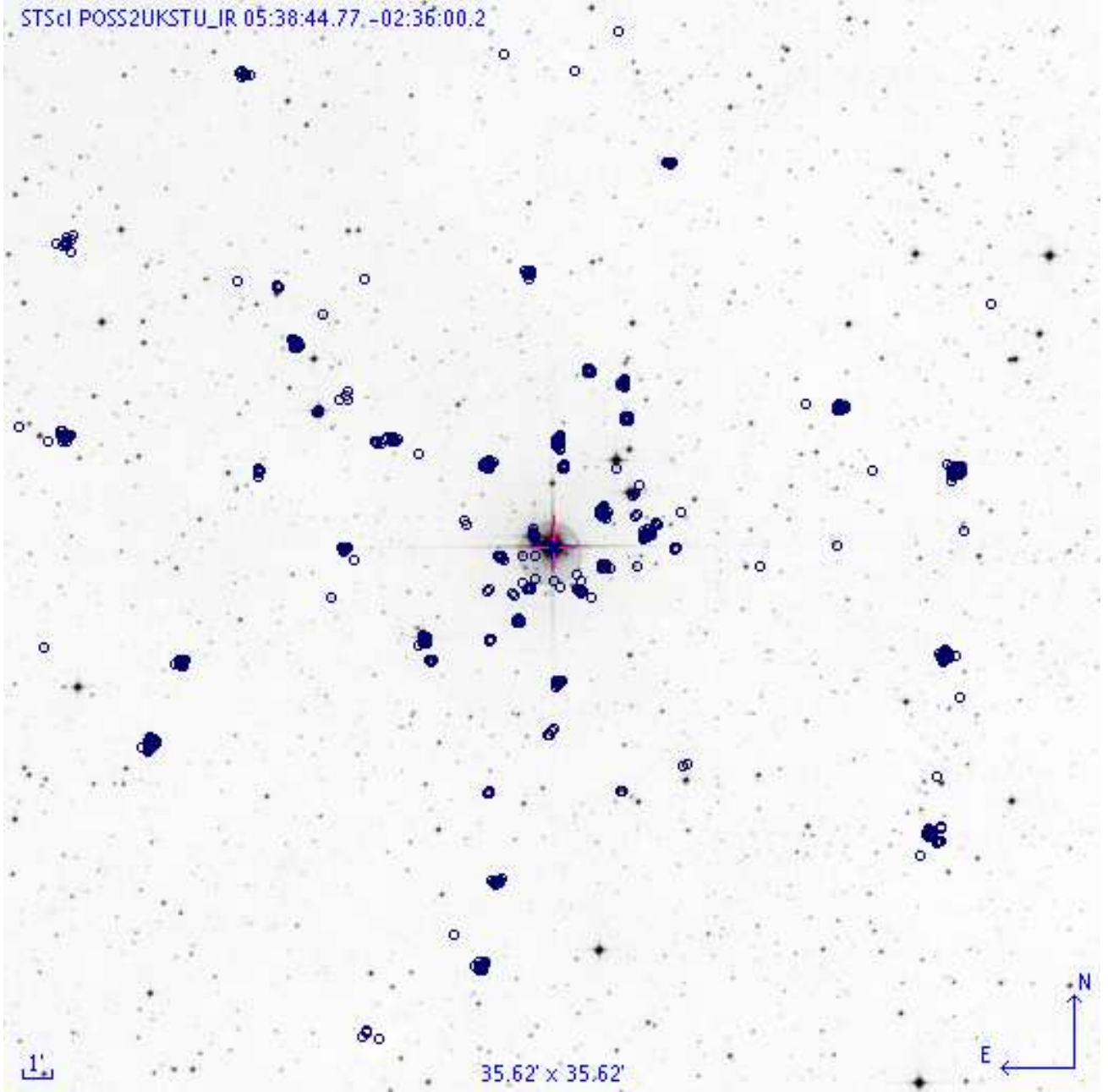


Fig. 1.— 1RXH events onto an I_N -band digitized image of the Palomar Observatory Sky Survey-II centered on σ Ori AF-B. Most of the events, indicated with small open circles, are associated to optical counterparts. Approximate size is $35 \times 35 \text{ arcmin}^2$, north is up, and east is left. See the electronic edition of the Journal for a color version of all our figures.

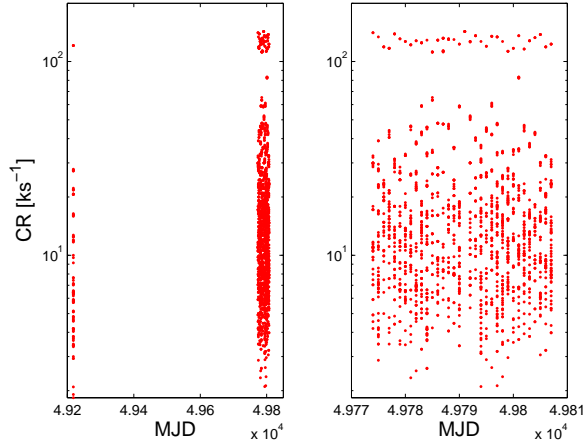


Fig. 2.— Net count error as a function of modified Julian date (CR vs. t_{MJD}). *Left:* The full interval (1992 Sep and 1995 Feb–Mar). *Right:* Zoom of the 1995 Feb–Mar interval. Data points above 100 ks^{-1} correspond to σ Ori AF–B.

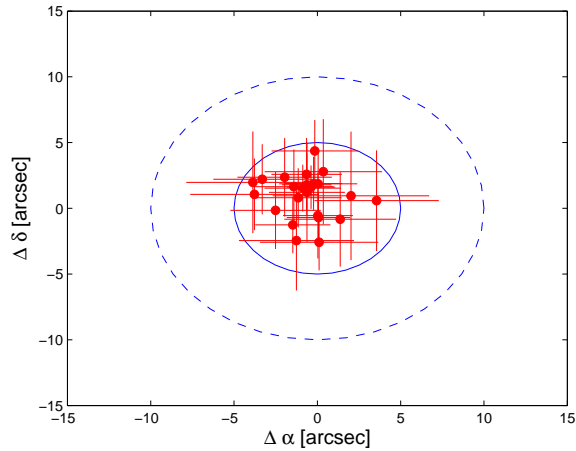


Fig. 3.— Separations between the 24 X-ray sources and their respective optical/near-infrared counterparts ($\Delta\delta$ vs. $\Delta\alpha$ diagram). Solid and dashed lines mark deviations of 5 and 10 arcsec, respectively. Actual maximum separations are about 4 arcsec.

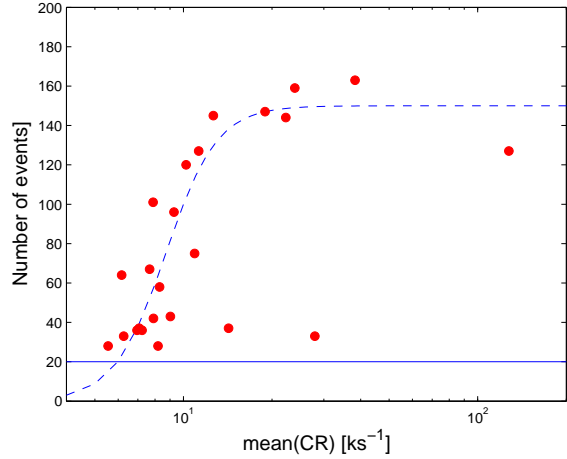


Fig. 4.— Number of 1RXH events associated to an X-ray source as a function of the mean net count rate (N vs. \overline{CR} diagram). The solid line is the lower limit at $N = 20$, while the dashed line is the sigmoid function described in the main text (Eq. 2).

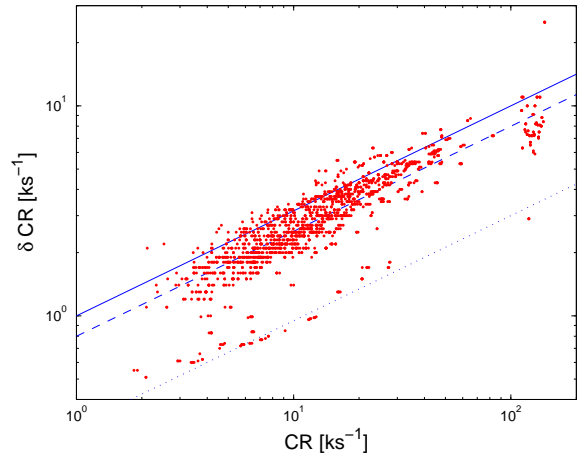


Fig. 5.— Mean error as a function of the net count error as tabulated by the ROSAT Team (2000) for all the 1RXH events (δCR vs. CR diagram). The solid, dashed, and dotted lines are for $\delta CR = 1.0 CR^{1/2}$, $0.8 CR^{1/2}$, and $0.3 CR^{1/2}$, respectively. The agglomerates of data points separated from the main data point cloud are for σ Ori AF–B ($CR > 100 \text{ ks}^{-1}$) and the 1992 Sep measurements (roughly overlapping with $\delta CR = 0.3 CR^{1/2}$).

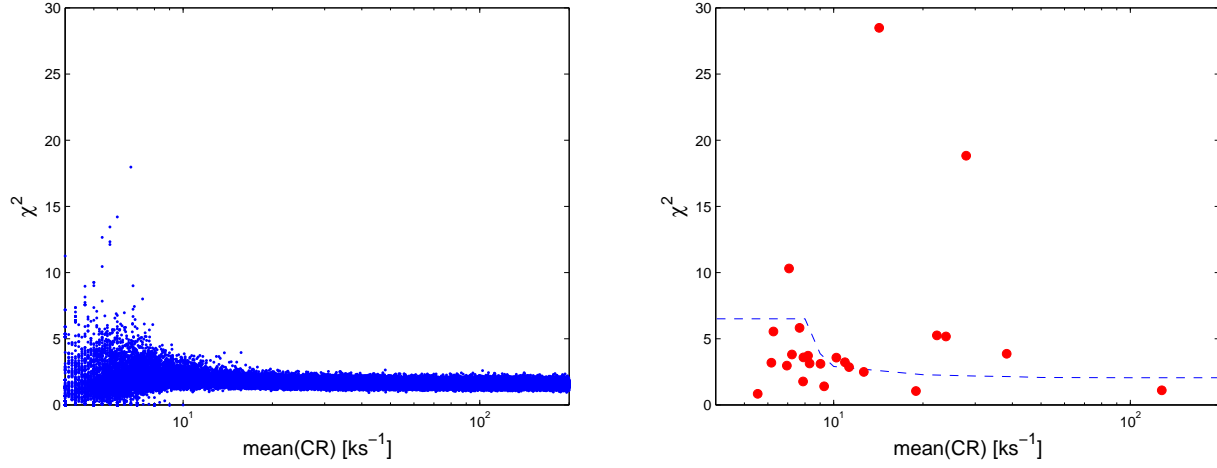


Fig. 6.— *Left*: χ^2 as a function of the mean net count rate (χ_j^2 vs. \overline{CR}_j diagram) for the 10^5 X-ray simulated series. *Right*: Same as left window, but for the 24 X-ray real series. X-ray sources above the dashed line have probabilities larger than 99% of being actual variables.

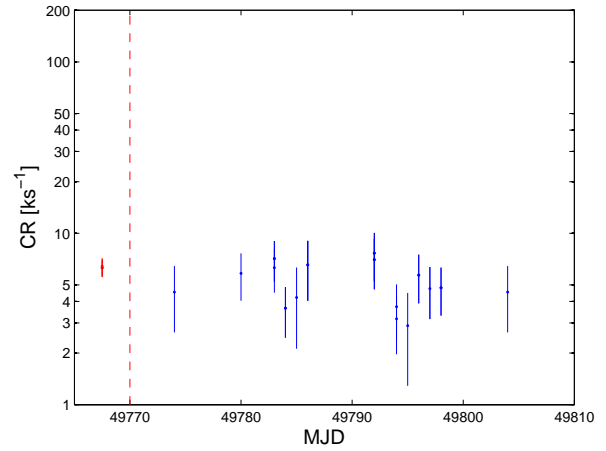
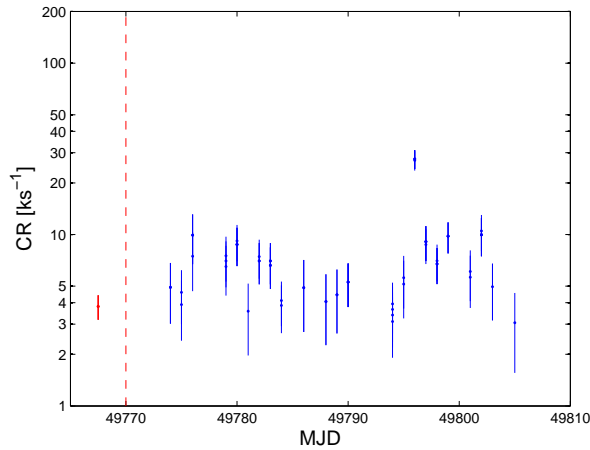
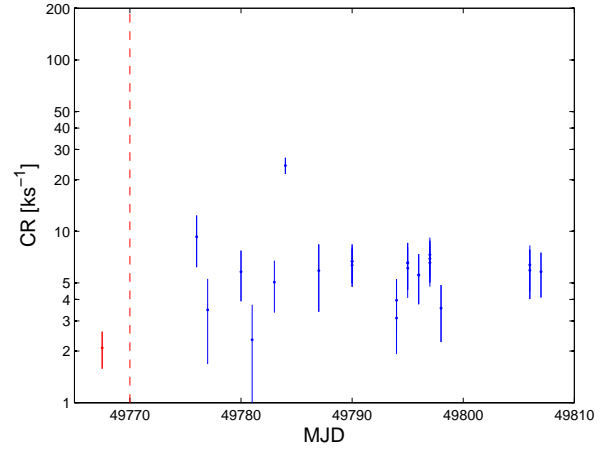
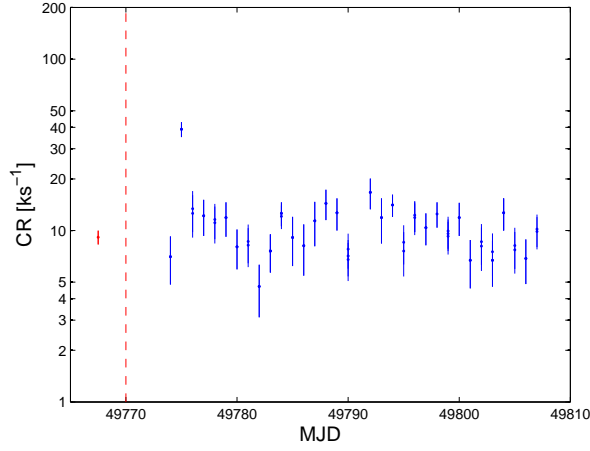
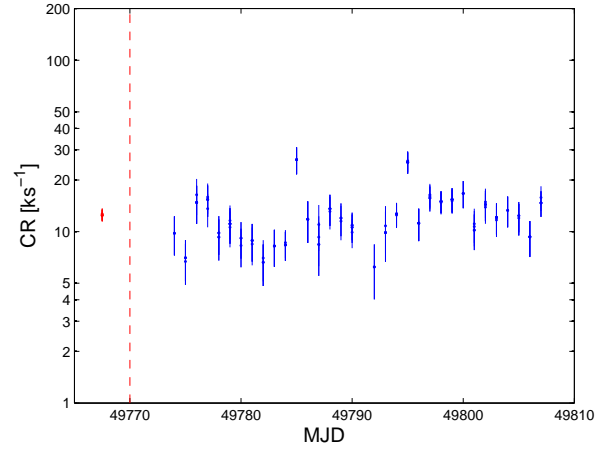
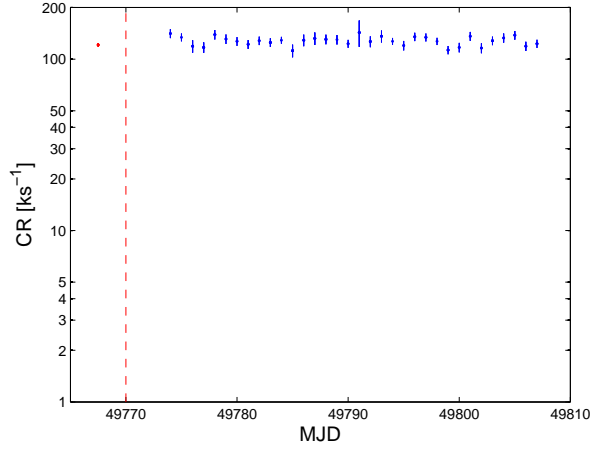


Fig. 7.— Time series of the 1RXH events associated to σ Ori AF-B, Mayrit 42062 (σ Ori E), and Mayrit 105249, from top to bottom. The isolated data points to the left of the vertical dashed line correspond to the 1992 Sep measurements; we have conveniently shifted these data points in the horizontal axis for a better visualization.

Fig. 8.— Same as Fig. 7, but for Mayrit 114305, Mayrit 156353, and Mayrit 157155.

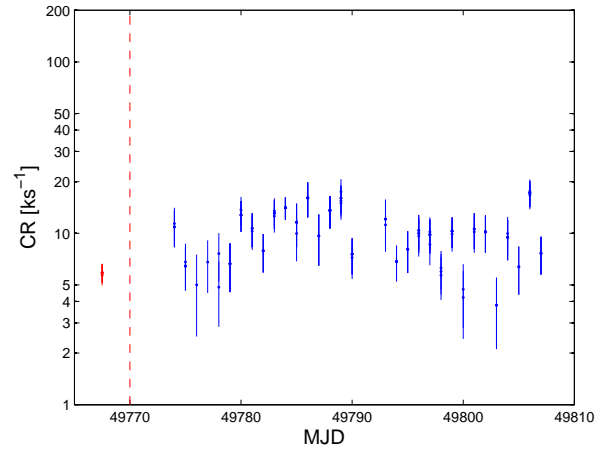
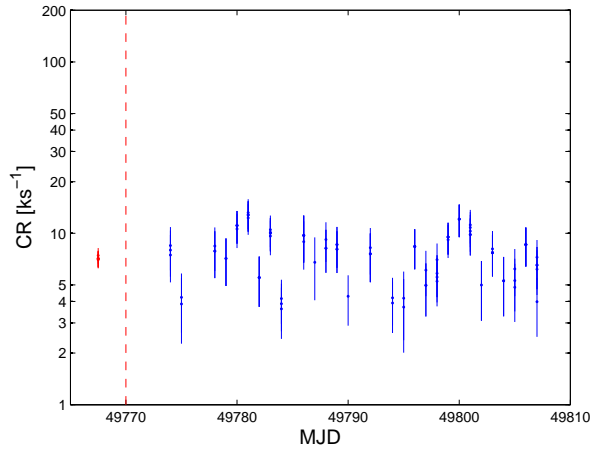
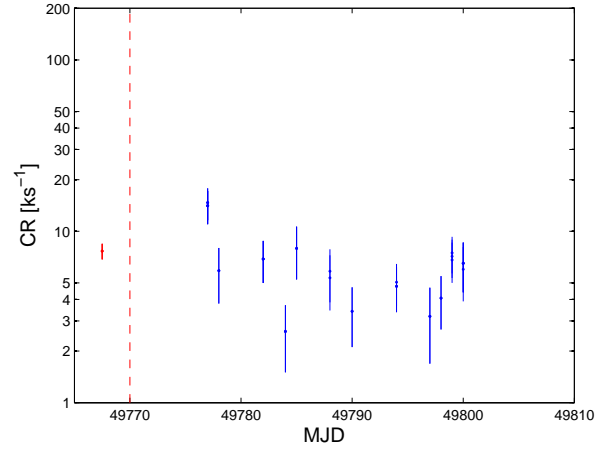
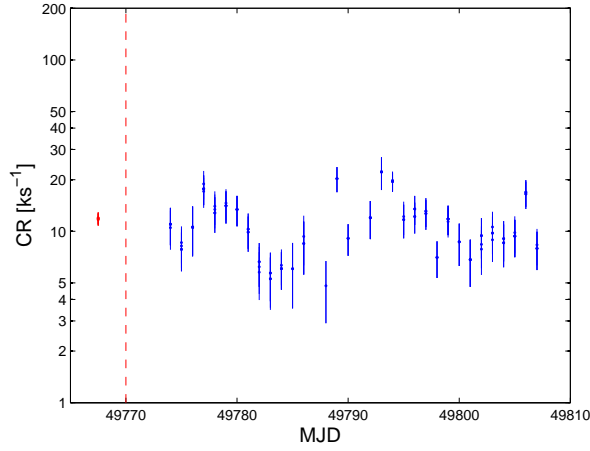
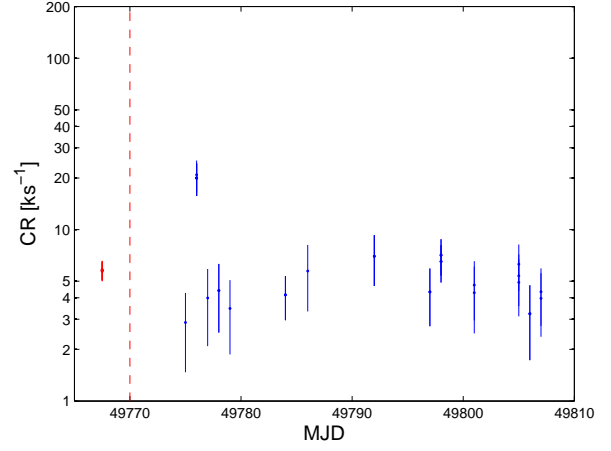
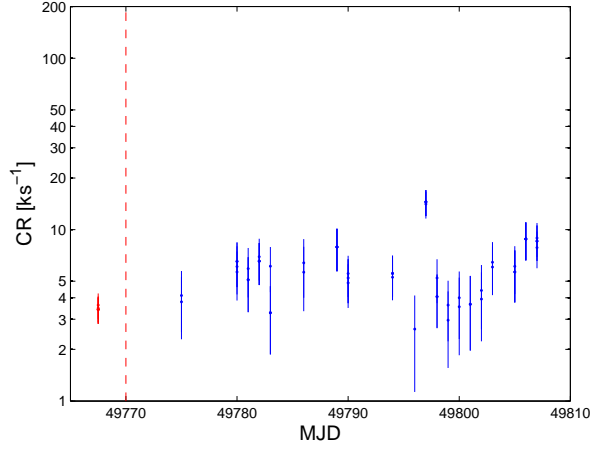


Fig. 9.— Same as Fig. 7, but for Mayrit 180277, Mayrit 203039, and Mayrit 207358.

Fig. 10.— Same as Fig. 7, but for Mayrit 260182, Mayrit 285331, and Mayrit 306125.

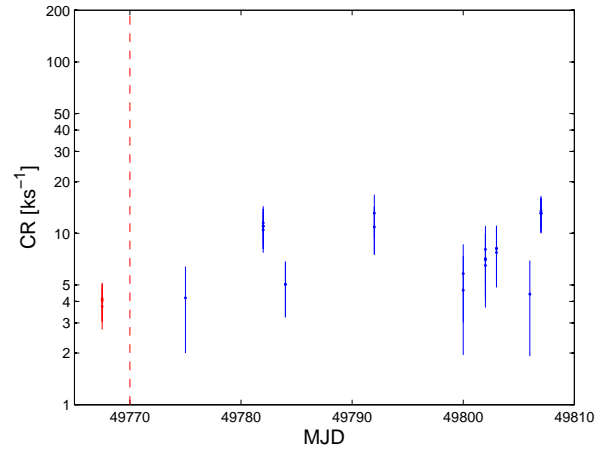
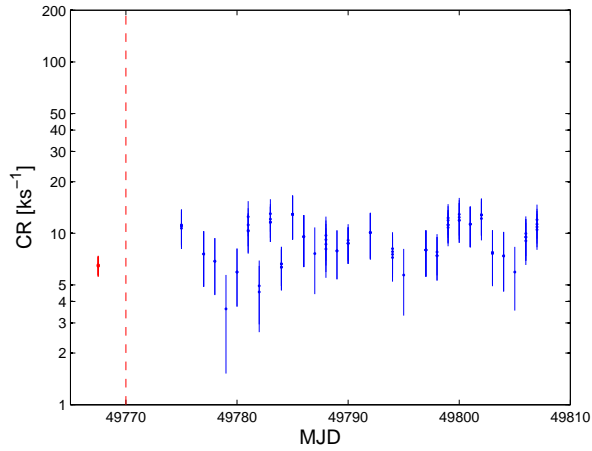
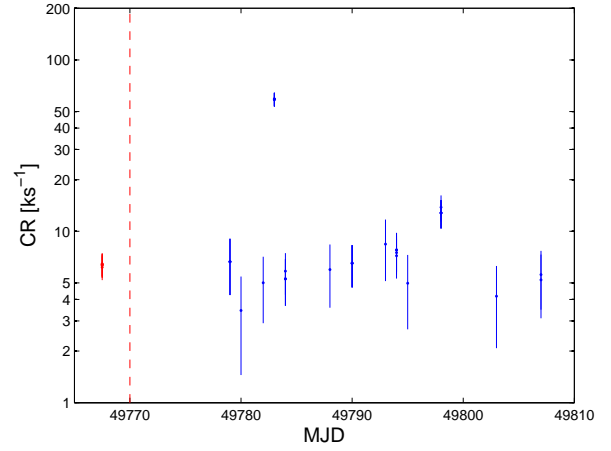
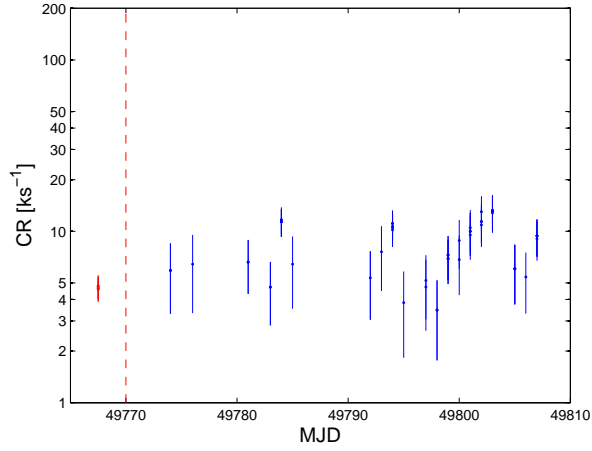
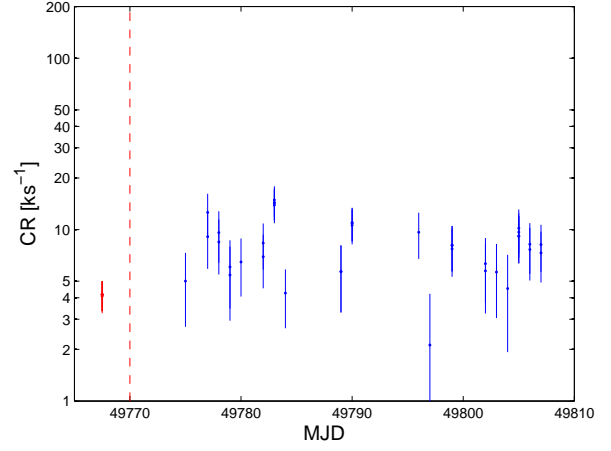
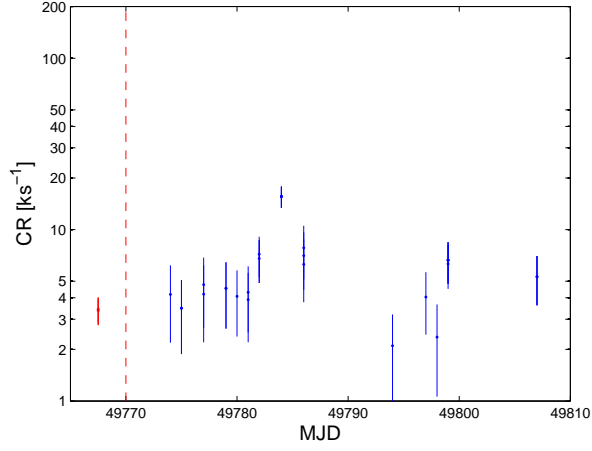


Fig. 11.— Same as Fig. 7, but for Mayrit 344337, Mayrit 528005, and Mayrit 615296.

Fig. 12.— Same as Fig. 7, but for Mayrit 634052, Mayrit 653170, and Mayrit 750107.

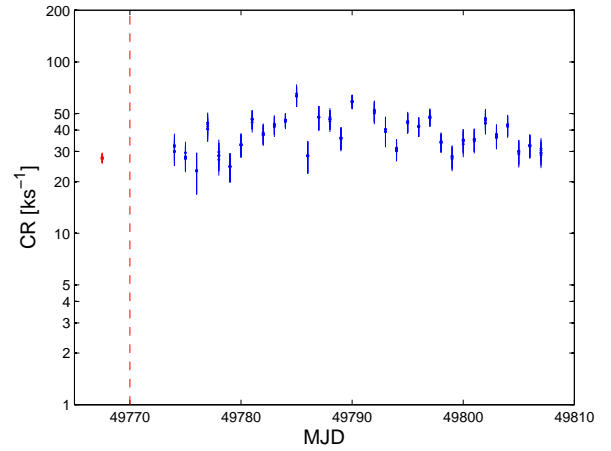
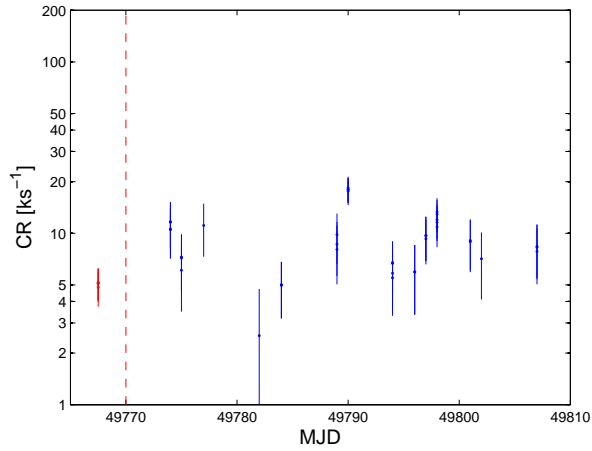
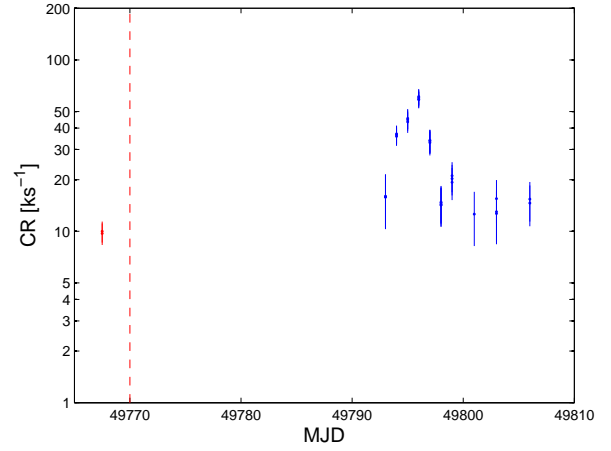
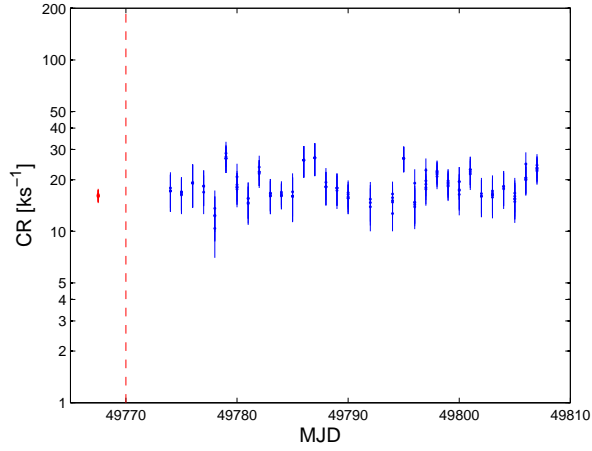
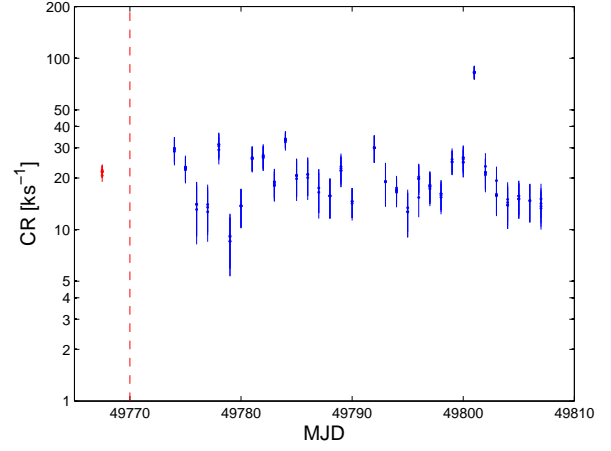
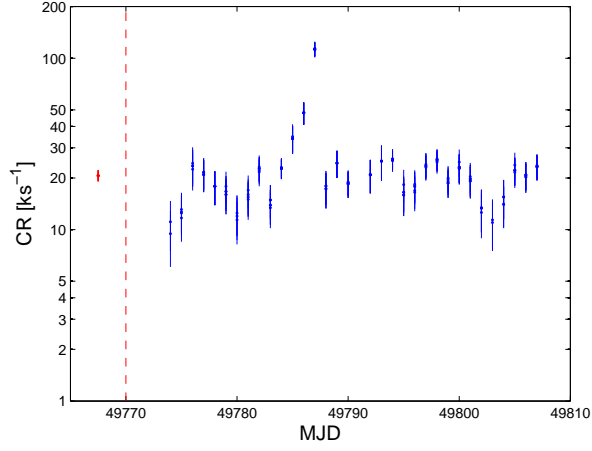


Fig. 13.— Same as Fig. 7, but for Mayrit 783254, Mayrit 789281, and Mayrit 822170.

Fig. 14.— Same as Fig. 7, but for Mayrit 863116, Mayrit 969077, and galaxy 2E 1456.